

Article

All-Nitrogen Cages and Molecular Crystals: Topological Rules, Stability, and Pyrolysis Paths

Konstantin P. Katin ^{1,2,*}, Valeriy B. Merinov ¹, Alexey I. Kochaev ³, Savas Kaya ⁴ and Mikhail M. Maslov ^{1,2}

¹ Department of Condensed Matter Physics, National Research Nuclear University “MEPhI”, Kashirskoe Sh. 31, 115409 Moscow, Russia; revan48@mail.ru (V.B.M.); MMMaslov@mephi.ru (M.M.M.)

² Laboratory of Computational Design of Nanostructures, Nanodevices, and Nanotechnologies, Research Institute for the Development of Scientific and Educational Potential of Youth, Aviatorov Str. 14/55, 119620 Moscow, Russia

³ Research and Education Center “Silicon and Carbon Nanotechnologies”, Ulyanovsk State University, 42 Leo Tolstoy Str., 432017 Ulyanovsk, Russia; a.kochaev@gmail.com

⁴ Faculty of Science, Department of Chemistry, Cumhuriyet University, Sivas 58140, Turkey; savaskaya1989@gmail.com

* Correspondence: kpkatin@yandex.ru

Received: 16 October 2020; Accepted: 3 November 2020; Published: 6 November 2020



Abstract: We combined ab initio molecular dynamics with the intrinsic reaction coordinate in order to investigate the mechanisms of stability and pyrolysis of $N_4 \div N_{120}$ fullerene-like nitrogen cages. The stability of the cages was evaluated in terms of the activation barriers and the activation Gibbs energies of their thermal-induced breaking. We found that binding energies, bond lengths, and quantum-mechanical descriptors failed to predict the stability of the cages. However, we derived a simple topological rule that adjacent hexagons on the cage surface resulted in its instability. For this reason, the number of stable nitrogen cages is significantly restricted in comparison with their carbon counterparts. As a rule, smaller clusters are more stable, whereas the earlier proposed large cages collapse at room temperature. The most stable all-nitrogen cages are the N_4 and N_6 clusters, which can form the van der Waals crystals with densities of 1.23 and 1.36 g/cm³, respectively. The examination of their band structures and densities of electronic states shows that they are both insulators. Their power and sensitivity are not inferior to the modern advanced high-energy nanosystems.

Keywords: nitrogen clusters; nitrogen fullerenes; topological rules; molecular crystals; density functional theory

1. Introduction

The formation of the N_2 molecule with the triple $N\equiv N$ bond from two isolated nitrogen atoms results in the release of a large amount of energy (≈ 10 eV [1]). Thus, nitrogen is considered as the primary component of the most high-energy compounds. Such compounds usually also contain carbon atoms that provide stability of the whole molecule framework decorated by oxygen-containing groups or other oxidants. RDX, HMX, and CL-20 are well-known examples of traditional high-energy structures with a carbon–nitrogen frame. In recent years, more advanced energy materials have been proposed with a similar carbon–nitrogen architecture [2–4].

The recent synthesis of nonmolecular nitrogen [5,6] has renewed research interest in all-nitrogen structures without carbon additives. Compared to carbon–nitrogen compounds, pristine nitrogen systems are more powerful and safer for the environment. In particular, closed full-nitrogen N_n cages with three-coordinated atoms and single N–N bonds are very attractive and environmentally friendly

oxygen-free fuels with an extremely high energy capacity. The transformation of single N–N bonds into the triple bond is a very exothermic process. The breakdown of N_n cages into N_2 molecules gives more than 50 kcal/mol per nitrogen atom [7]. However, in practice, N_n cages possess low stability and have not yet been synthesized and measured. Unlike carbon fullerenes, fully nitrogen cages do not retain their structure under ambient conditions, since they are energetically unfeasible compared to N_2 molecules. In addition, the activation energies of their decay processes are rather low. Thus, most N_n cages can be prepared and stabilized only at extremely high pressures, similar to recently obtained forms of nonmolecular nitrogen [5,6]. The introduction of carbon atoms, oxygen, or other atoms into the nitrogen cages leads to more stable structures [3,4,8], which, however, are not as efficient and environmentally friendly as all-nitrogen hypothetical analogs [7,9].

Many researchers have looked at the structures of N_n cages in order to find some that are stable enough to be used in practice. All-nitrogen N_4 [10], N_6 [11], N_8 [12], N_{10} [9], N_{12} [9,13], N_{14} [14], N_{16} [14], N_{18} [15], N_{20} [9,16], N_{24} [17], N_{30} [17], and N_{36} [17] structures turned out to be local energy minima in the systems' configuration spaces. A genetic algorithm was recently applied to search for configurations of global minima of N_n ($n = 3 \div 10$) clusters [18]. Among huge N_n cages with $n > 36$, only a limited number of systems were considered. All of them are tubular clusters similar to nanotubes [19–21]. Unexpectedly, the N_{60} cluster with an I_h symmetry (the nitrogen analog of the traditional C_{60} fullerene) was found to be unstable even at zero temperature [22]. Low kinetic stability can be considered as the Achilles heel of all previously studied systems, even if they were true energy minima in the configuration space.

In the presented paper, we carry out a systematic study of the structure and stability of N_n fullerene-like cages. Our goal is to identify the general relationships between the topology and stability of nitrogen buckyballs. Unlike previous calculations, we focus on the pyrolysis mechanisms and the corresponding activation barriers, rather than on the relative formation energies of the structures under consideration. We identify the most stable N_n cages, explain the reasons for their stability, and investigate the possibilities of their crystallization.

2. Computational Details

Finite-size nitrogen cages were simulated in the frame of the density functional theory with the B3LYP functional [23,24] and 6-311G(d,p) basis set [25]. GAMESS-2013 software [26] was used for optimizing stable and transition states, calculating molecules' vibrational eigenmodes, and following along the intrinsic reaction coordinates. Default numerical thresholds were applied in all cases. Thermodynamic quantities (Gibbs energy and enthalpy) were calculated from molecules' eigenfrequencies in the frame of ideal gas approximation. Binding energies E_b of N_n cages concerning molecular nitrogen were calculated as

$$E_b = \frac{1}{n}(E(N_n \text{ cage}) - 0.5nE(N_2 \text{ molecule})) \quad (1)$$

The activation Gibbs energy ΔG , activation enthalpy ΔH , and energy barrier ΔU were obtained as the differences of the corresponding values for transition and initial configurations of nitrogen cages. The lifetime of a molecule t before the thermal decomposition at a temperature T was estimated using the Arrhenius law:

$$t = (Ag)^{-1} \exp\left(-\frac{\Delta U}{kT}\right), \quad (2)$$

where k is the Boltzmann constant. Frequency factors A were defined in accordance with the Vineyard's rule [27]

$$A = \frac{\prod_{i=1}^{3n-6} \omega}{\prod_{i=1}^{3n-7} \omega'}, \quad (3)$$

where ω and ω' are real eigenfrequencies at stable and transition states, respectively. It should be noted that the imaginary eigenfrequency of the transition state is not included in the multiplication.

Degeneracy factor g is equal to the number of equivalent decay paths ($g > 1$ for high-symmetry N_n cages).

Ab initio molecular dynamics was carried out using a high-performance GPU-based TeraChem 1.9 package [28–31] with the same B3LYP/6-311G(d,p) level of theory. The initial atomic displacements and velocities were generated in accordance with the desired temperature. During the simulation, the given temperature was maintained by the Langevin thermostat [32]. The time step for all simulations was 0.1 fs, which was sufficient for taking into account all molecular vibrations correctly. The systems' dynamical trajectories were visualized using the ChemCraft 1.8 program [33].

To study the geometry and electronic structure properties of crystals that consist of the nonmolecular nitrogen systems, we used another density functional theory approach and its implementation in the QUANTUM Espresso 6.5 program package [34,35]. The generalized gradient approximation (GGA) in the Perdew–Burke–Ernzerhof (PBE) functional form for the exchange-correlation energy [36] and the projector-augmented-wave (PAW) method for the electron-ion interaction [37,38] were used to perform the calculations. The value of the cut-off energy for the plane-wave basis set was chosen as 120 Ry (1632 eV). The weak van der Waals interactions between the noncovalently bound nitrogen atoms were taken into account by using the D3 Grimme dispersion corrections [39]. The geometry optimization of the nitrogen crystal was performed without any symmetry constraints until the Hellman–Feynman forces acting on the atoms became smaller than 10^{-6} hartree/bohr. Supercell parameters were also optimized. The Brillouin zone integrations were performed by using the Monkhorst–Pack k-point sampling scheme [40] with the $8 \times 8 \times 8$ mesh grid. For the non-self-consistent field calculations, the k-point grid size of $24 \times 24 \times 24$ was used. The Methfessel–Paxton smearing [41] was used for the geometry relaxation with a smearing width of 0.02 eV. Still, for the calculations of the electronic density of states, the Böchl tetrahedron method [42] was employed. The electronic structure properties were elucidated through the analysis of the sample band structure and its electronic density of states.

3. Results and Discussion

3.1. The First Insight on the Bicyclic Hydronitrogen Molecules

Hypothetical bicyclic hydronitrogen molecules are the smallest possible systems containing adjacent nitrogen rings with the single N–N bonds. We constructed $N_{10}H_8$, N_9H_7 , N_8H_6 , N_7H_5 , and N_6H_4 naphthalene-like molecules with hexagon/hexagon, hexagon/pentagon, pentagon/pentagon, pentagon/square, and square/square interfaces, respectively (see Figure 1a). Unlike their carbon counterparts, these molecules do not remain flat during geometry optimization due to the sp^3 -hybridization of nitrogen, which differs from carbon bicycles in which sp^2 hybridization occurs.

We found that the hexagon/pentagon and the pentagon/pentagon were the only stable configurations with positive eigenfrequencies. Other structures are not true energy minima. Potential energy paths corresponding to the breaking of joint hexagon/pentagon and pentagon/pentagon bonds are shown in Figure 1b,c (the energy barriers are 0.58 and 0.47 eV, respectively). Therefore, the pentagon/pentagon interface seems to be the most suitable. The hexagon/pentagon interface possesses lower stability, while the adjacent hexagons lead to complete instability. It should be noted that the carbon structures exhibit the opposite behavior, avoiding adjacent pentagons according to Kroto's isolated pentagon rule [43].

However, bicyclic molecules can only give qualitative insight into the stability of all-nitrogen cages. They do not reproduce local curvature effects, which is especially crucial for small cages, and other effects such as three-dimensional aromaticity. Moreover, hydrogen passivation distorts the charge distribution in the nitrogen rings. Thus, the conclusions made from the analysis of bicyclic nitrogen-containing molecules should be verified on more suitable all-nitrogen systems.

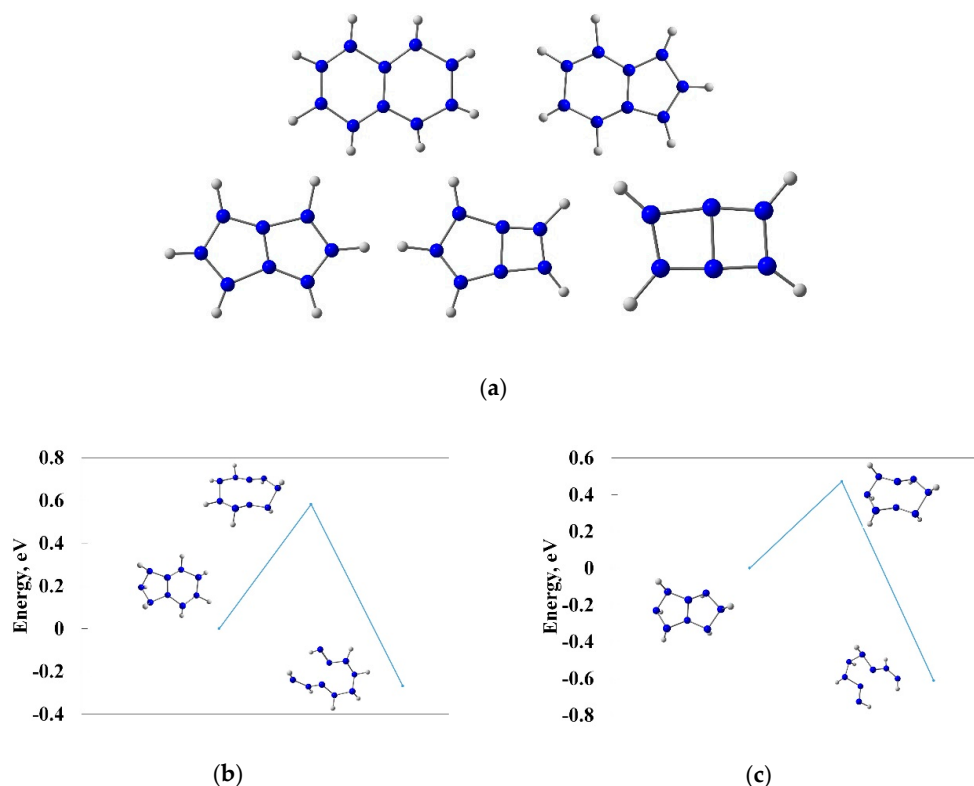


Figure 1. Hypothetical bicyclic hydronitrogen molecules N_{10}H_8 , N_9H_7 , N_8H_6 , N_7H_5 , and N_6H_4 (a). Energy diagram of the N–N bond rupture, which is typical for adjacent rings (b,c).

3.2. Nitrogen Cages with Adjacent Hexagons

As a next step, we constructed nitrogen analogs of low-energy isomers of carbon fullerenes from C_{20} to C_{120} , created using the FULLERENE 4.5 code [44]. All possible isomers C_{20} – C_{32} , as well as all low-energy isomers C_{34} – C_{120} , included in the Tomanek database [45], were used as the initial sample geometry for all-nitrogen cages. It should be noted that the typical length of a single N–N bond (1.45 \AA) is close to the lengths of C–C bonds in the fullerenes under consideration. However, all the corresponding N_n systems lose their fullerene-like shape when the geometry is optimized. The only exceptions were the clusters N_{20} and N_{24} , which did not contain adjacent hexagons. For all other cages, optimization leads to the breaking of those N–N bonds that are common for the neighboring hexagons, and the subsequent destruction of the nitrogen cage. Thus, we conclude that the presence of adjacent hexagons leads to cage instability.

The only known N_n cages with the adjacent hexagons are tubular structures, first considered in Refs. [19–21]. The structure of the first members belonging to N_n tubular systems is shown in Figure 2a. The extremely small diameters of these tubes provide stability due to the curvature effects and concave hexagon shapes. It should be noted that the large diameter N_n tubular structures are unstable [46]. We tested the stability of the tubular systems shown in Figure 2 using ab initio molecular dynamics (AIMD) at $T = 700 \text{ K}$ for one picosecond. We observed their decomposition into N_2 molecules, and short N_n chains ($n = 3 \div 7$) started with breaking the adjacent sides of the neighboring hexagons. We conclude that their stability is too low even for their identification. Such nitrogen nanostructures can hardly be used for any practical applications under ambient conditions. Our calculations confirm that unlike carbon, nitrogen avoids the formation of adjacent hexagonal rings. It should be noted that at the moment, compounds containing adjacent N_6 rings have not yet been experimentally synthesized.

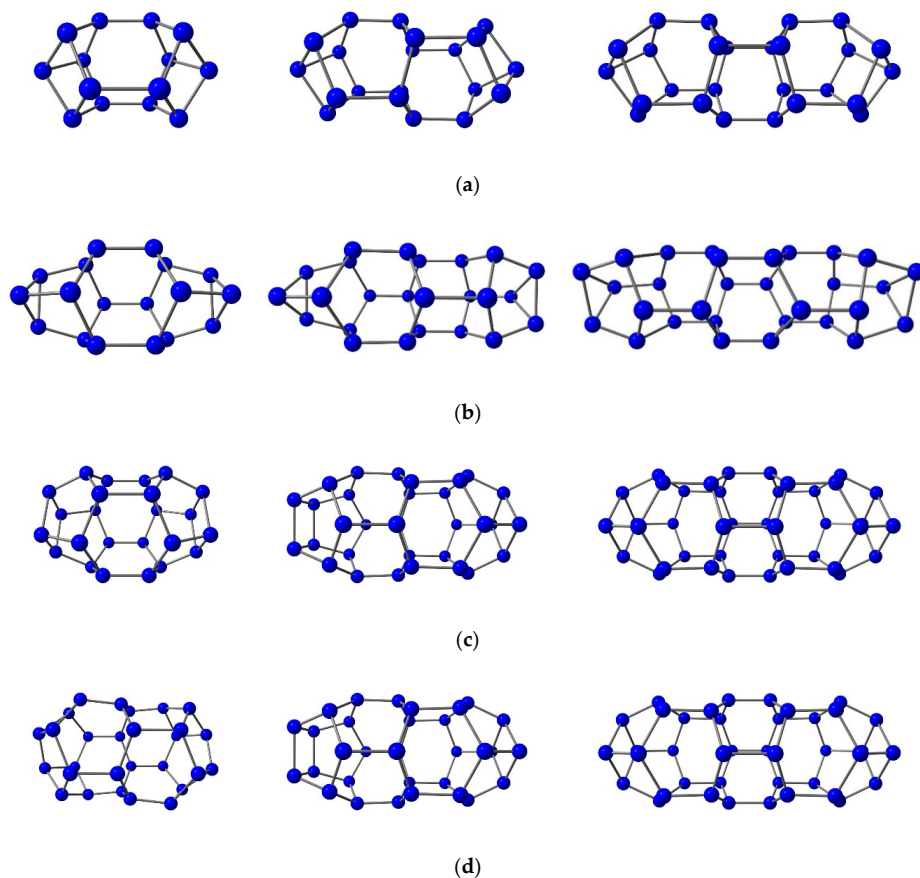


Figure 2. Examples of tubular nitrogen clusters with adjacent hexagons. Nitrogen nanotubes with wall surface formed by three hexagons that contain caps at the ends closed by one (a) and three (b) nitrogen atoms. Nitrogen nanotubes with wall surface formed by four hexagons that contain caps at the ends closed by four (c) and two (d) nitrogen atoms.

3.3. Nitrogen Cages without Adjacent Hexagons

A large number of hexagons on the fullerene surface leads to a small curvature and large size of the system. To avoid adjacent pentagons, carbon clusters C_n should be sufficiently large ($n \geq 60$). In contrast, the hexagons on the surface of nitrogen clusters (if any) should be separated by pentagons or smaller polygons, and therefore the fraction of the hexagons should be low. Thus, stable nitrogen clusters N_n should have a significant curvature and small size ($n \leq 24$). Inspired by small carbon fullerenes and fullerene-like cages (including tetrahedranes, prismanes, nonclassical fullerenes, etc.), we constructed the corresponding nitrogen structures. All the nitrogen cages satisfying the isolated hexagon rule that are true local energy minima are presented in Figure 3. The kinetic stability of these systems was investigated using AIMD at $T = 700$ K for one picosecond. Only the five smallest nitrogen clusters, labeled as Figure 3a–e, conserved their identity during the AIMD simulation (their pyrolysis mechanisms will be described in more detail in the next subsection). Larger clusters are decomposed; therefore, they should be considered as low-stable systems. It should be noted that N–N bonds in all truly stable and low-stable cages are longer than 1.4 Å, indicating that the bond type is single. The maximum lengths of N–N bonds, binding energies E_b , and differences between the lowest unoccupied and the highest occupied molecular orbitals (HOMO-LUMO gaps) for all cages are shown in Figure 4a–c. It should be noted that all these characteristics (and their values) do not correlate with the kinetic stability and, therefore, cannot be used as indicators of stable systems. Quantum-chemical descriptors calculated from the energies of the frontiers orbitals are shown in Figure S1 in Supplementary Materials. None of the descriptors show a direct correlation with the kinetic stability of the corresponding nitrogen cage.

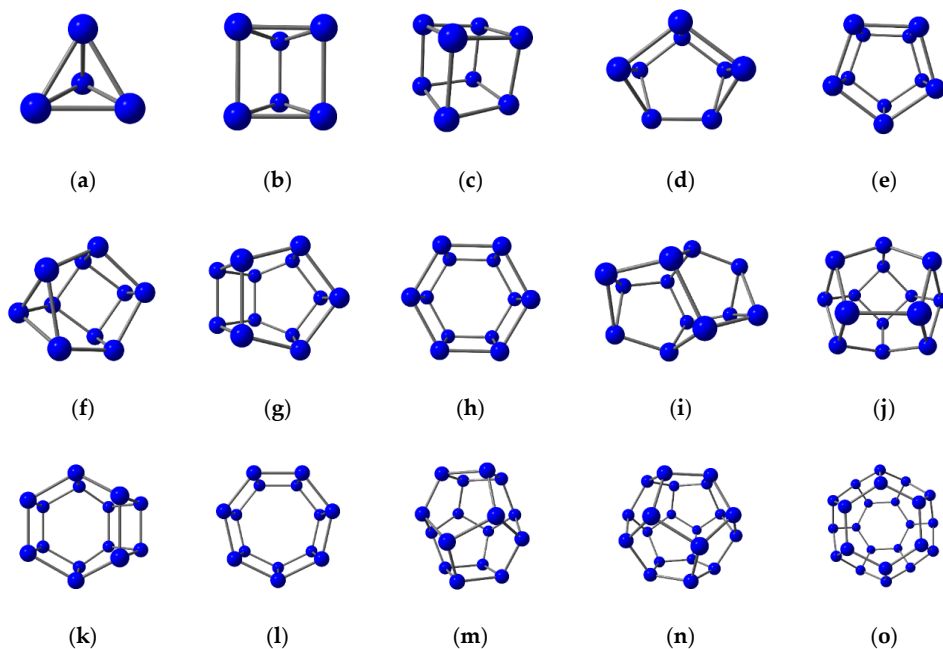


Figure 3. Nitrogen cage structures without the adjacent hexagons. Atomic structures (a–e) are stable, while other systems (f–o) possess low stability.

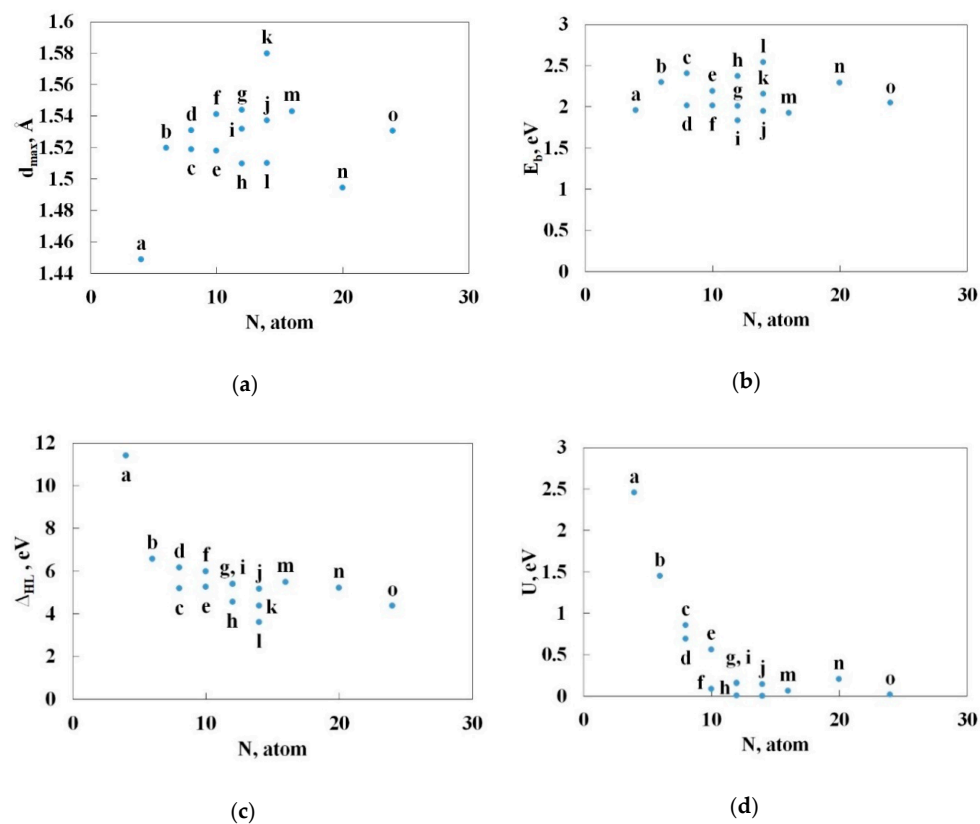


Figure 4. The maximum lengths of N–N bonds (a), binding energies E_b (b), differences between the lowest unoccupied and the highest occupied molecular orbitals (HOMO-LUMO gaps) (c), and activation barriers U (d) for corresponding nitrogen cages presented in Figure 3. Letter designations correspond to designations in Figure 3.

To get a complete understanding of the origin of the stability of nitrogen cages, we analyzed the mechanisms of their pyrolysis. We adopted the reaction mechanism from the ab initio molecular dynamics. Knowing the reaction mechanism, we performed an intrinsic reaction coordinates calculation. The preliminary transient geometries obtained from the AIMD simulations were further optimized to find the true transient configurations (the corresponding atomic coordinates are collected in Supplementary Materials). Energy barriers U are shown in Figure 4d. One can define two distinct groups of clusters: “stable” with $U > 0.5$ eV and “low-stable”, characterized by the value of $U < 0.25$ eV. The analysis of the energy barriers confirms the previous AIMD simulation, where the same stable clusters were distinguished.

3.4. Pyrolysis of the Most Stable Nitrogen Cages and the Possibility of Further Stabilization

The pyrolysis of five “stable” nitrogen cages was analyzed in more detail. Rate-dependent reaction steps, the corresponding transition states, and products are shown in Figure 5. Thermodynamic descriptors (activation enthalpies and Gibbs activation energies) at various temperatures are collected in Table 1. These descriptors weakly depend on temperature for all clusters, since the initial and transition configurations are not so different, and their vibrational energies and entropies slightly differ from each other.

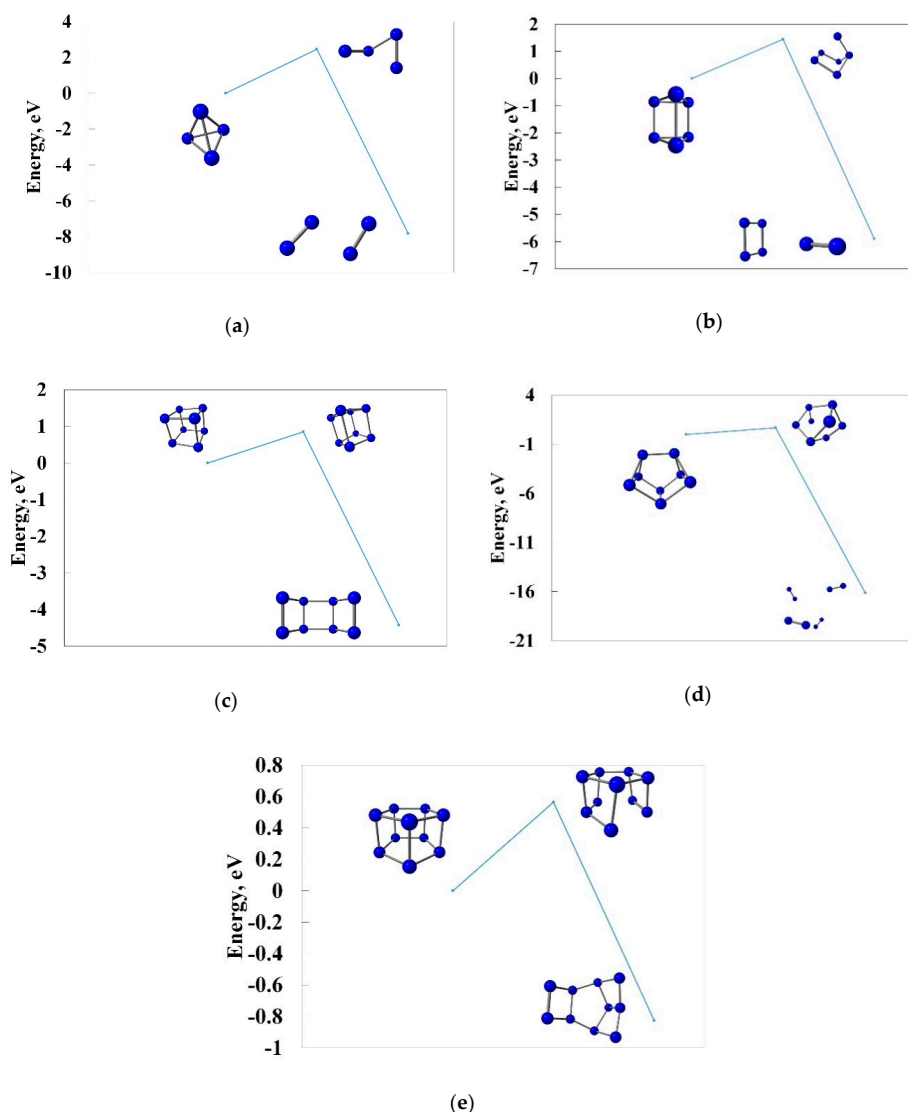


Figure 5. Pyrolysis mechanisms of stable nitrogen clusters N₄ (a), N₆ (b), N₈ (c), N₈ (d), and N₁₀ (e).

Table 1. Characteristics of the decay of “stable” nitrogen cages N_n : energy barriers U , degeneracy factors g , imaginary frequencies of the transition state ω , activation enthalpies ΔH , activation Gibbs energies ΔG , and mean lifetimes t at different temperatures.

	U (eV)	g	ω (cm^{-1})	ΔH (kJ/mol)			ΔG (kJ/mol)			t (s)		
				300 K	400 K	500 K	300 K	400 K	500 K	300 K	400 K	500 K
N_4 (a)	2.46	4	664.1i	230.5	230.5	226.1	229.1	228.7	228.3	9.6×10^{26}	4.6×10^{16}	2.9×10^{10}
N_6 (b)	1.45	2	721.1i	132.0	132.1	132.0	130.7	130.2	129.8	1.6×10^{10}	1.3×10^4	3.0
N_8 (c)	0.85	6	1658.4i	70.6	71.4	71.7	65.8	64.1	62.3	6.1×10^{-2}	1.6×10^{-5}	1.2×10^{-7}
N_8 (d)	0.69	4	746.4i	58.7	59.0	59.0	55.1	53.9	52.6	5.1×10^{-4}	6.6×10^{-7}	1.2×10^{-8}
N_{10} (e)	0.56	10	566.7i	47.8	47.9	47.6	46.1	45.5	45.0	4.3×10^{-6}	1.8×10^{-8}	6.9×10^{-10}

According to Table 1, only N_4 and N_6 clusters have a reasonable lifetime at room temperature. Thus, they should be considered as the most promising high-energy-density structures. More extensive systems need additional stabilization with low temperature or high pressure. According to our previous simulations, small nitrogen clusters can be substantially stabilized via spatial constraints [47] (for example, inside porous materials or carbon cages [48]). Due to the compact shape of small nitrogen clusters, spatial confinement can increase their decomposition activation barrier by 0.5 eV or more [48], which is sufficient to stabilize them at room temperature but hardly useful at higher temperatures.

3.5. Van der Waals Nitrogen Crystals

Recently, some crystal structures have appeared based on the chains N_6 [49] and N_8 [50], as well as other single-bonded all-nitrogen systems [51,52]. According to the above calculations, the N_4 and N_6 clusters are very stable and can be considered as an alternative to nitrogen chains. Their activation barriers are even higher than the corresponding values for experimentally observed highly strained hydrocarbons (for example, tetrahedrane C_4H_4 [53] or polymethylcubanes $C_8H_q(CH_3)_{8-q}$ [54]). Thus, N_4 and N_6 are the most suitable candidates for building blocks for the high-energy-density crystals.

There are many algorithms for predicting the crystal structure. The most famous of them are USPEX [55] and CALYPSO [56]. However, they seem rather excessive for the construction of relatively simple molecular crystals in which the N_4 and N_6 cages conserve their shape. Isolated nitrogen cages bind in such crystals due to the weak Van der Waals interaction. Instead, we constructed three initial lattices for each crystal (sc, bcc, and fcc) and optimized atomic positions along with lattice vectors without any symmetry constraints. Then, the crystals with the lowest potential energy were considered. Their crystallographic parameters are summarized in Table 2. Their band structures and electron densities of states are shown in Figure 6. Coordinates of the atomic positions are available in Supplementary Materials.

Table 2. Characteristics of the N_4 and N_6 molecular crystals: crystallographic parameters, density p , the heat of detonation Q , detonation velocity D , adiabatic exponent Γ , detonation pressure P , and typical impact sensitive parameter $h_{50\%}$.

Crystallography Data		p (g/cm ³)	Q (cal/g)	D (m/s)	Γ	P (Kbar)	$h_{50\%}$ (cm)
N_4	$a = 5.3 \text{ \AA}, b = c = 4.6 \text{ \AA}$ $\alpha = 70^\circ, \beta = \gamma = 55^\circ$	1.23	2679.3	7550	3.1	170.4	28.7
N_6	$a = 5.7 \text{ \AA}, b = 4.8 \text{ \AA}, c = 6.0 \text{ \AA}$ $\alpha = 67.5^\circ, \beta = 50.6^\circ, \gamma = 54.4^\circ$	1.36	3219.1	8310	3.2	220.9	28.7

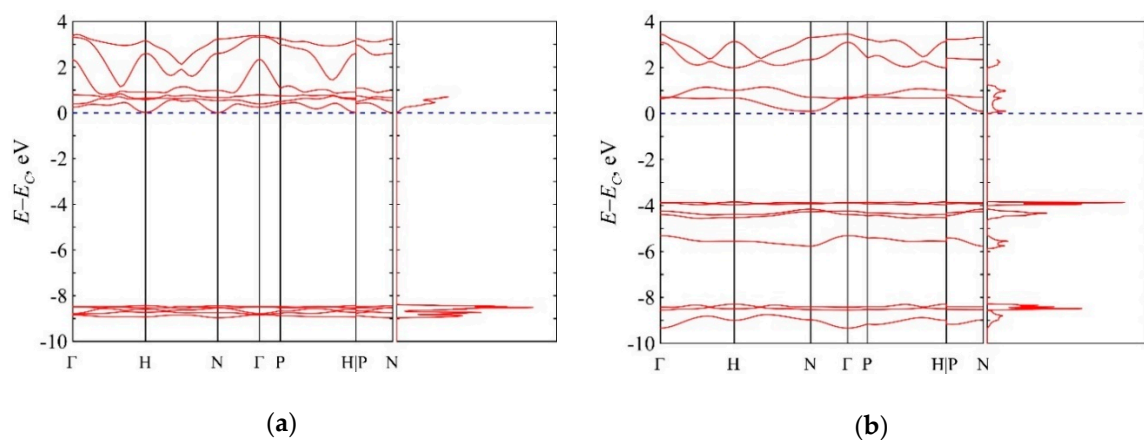


Figure 6. Band structures (left) and electron densities of states (right) for the most stable molecular crystals N_4 (a) and N_6 (b). Energy EC denotes the bottom of the conduction band.

Assuming the detonation of these crystals with the release of gaseous N_2 , we estimated the heat of detonation Q as the difference in energies between crystals and nitrogen molecules. In addition, the characteristics of detonation (detonation velocity D , adiabatic exponent Γ , detonation pressure P) can be estimated from Q and crystal density p in accordance with the Xiong empirical rules [57], which, in our case, have the following forms:

$$D\left[\frac{m}{s}\right] = 67.6 \left(Q\left[\frac{cal}{g}\right]\right)^{0.5} + 3300.2p\left[\frac{g}{cm^3}\right], \quad (4)$$

$$\Gamma = 1.25 + 3.8 \left(1 - \exp\left(-0.546p\left[\frac{g}{cm^3}\right]\right)\right), \quad (5)$$

$$P[kbar] = p\left[\frac{g}{cm^3}\right] \left(D\left[\frac{m}{s}\right]\right)^2 \cdot 10^{-5} / (1 + \Gamma) \quad (6)$$

The calculation results are also shown in Table 2. It can be seen that the proposed all-nitrogen crystals have detonation parameters comparable to conventional high-energy materials.

It is more difficult to predict the impact sensitivity of high-energy crystals, which can be characterized by the typical parameter $h_{50\%}$ [58]. Many approaches have been proposed based on the frontier orbitals, electrostatic potentials, and other electronic characteristics [58,59]. However, their accuracy for the novel compounds is rather questionable [60]. Rice and Hare indicated that determining the $h_{50\%}$ based on the Q value is preferable [60]. Here, we adopted the following model [59]:

$$h_{50\%}[cm] = 27.8 + 0.11 \exp\left(-11.08\left(Q\left[\frac{cal}{g}\right] - 1.66\right)\right) \quad (7)$$

High Q values result in a negligibly small second term, so the formula gives a satisfactory $h_{50\%}$ value of 27.8 cm for both crystals (see Table 2), which is two times higher than the corresponding value for ε -CL-20 (12 cm [61]). It should be noted that this is only a qualitative estimation of impact sensitivity. However, this confirms the potential applicability of the nitrogen crystals as high-energy materials.

4. Conclusions

In this paper, we analyzed the structure and stability of all-nitrogen fullerene-like clusters and the molecular crystals based on them. According to the formulated topological rule, confirmed by density functional theory calculations, only small nitrogen cages with single N–N bonds are stable. In terms of stability, they can compete with actively studied nitrogen chains. An increase in cage size always

leads to a sharp decrease in its stability. Thus, the range of nitrogen cages is significantly limited. Larger structures can be formed from small building blocks due to noncovalent interactions.

However, our conclusions are valid only for convex cages. We admit that the concave shape of the nitrogen structure can contribute to its stability. However, the curvature of such a hypothetical construction must change its shape many times in order to avoid large convex regions. The study of such astralene-like structures is beyond the scope of this study. We believe that the topological rules presented here will facilitate the further search for new clusters and crystals of nitrogen.

Like strained hydrocarbon frameworks, small nitrogen clusters are stable enough to form molecular crystals. The performed analysis of the two most promising all-nitrogen structures confirmed their applicability as competitive, high-energy materials.

Supplementary Materials: The following are available online at <http://www.mdpi.com/2079-3197/8/4/91/s1>, Figure S1: The chemical potential (a), hardness (b), softness (c), and electrophilicity index (d) versus the number of nitrogen atoms in the system obtained at the DFT/B3LYP/6-311G(d,p) level of theory. Letter designations correspond to designations in Figure 3 of the main text. Table S1: Optimized cartesian coordinates of nitrogen nanosystems considered. Letter designations correspond to designations in Figure 3 of the main text.

Author Contributions: K.P.K.: conceptualization; investigation; methodology; resources; software; writing—original draft; V.B.M.: data curation; formal analysis; investigation; software; validation; visualization; writing—review and editing; A.I.K.: formal analysis; investigation; software; validation; visualization; writing—review and editing; S.K.: formal analysis; investigation; software; validation; visualization; writing—review and editing; M.M.M.: conceptualization; funding acquisition; investigation; methodology; project administration; resources; software; writing—original draft. All authors have read and agreed to the published version of the manuscript.

Funding: The reported study was funded by RFBR according to the research project No. 18-32-20139 mol a_ved.

Conflicts of Interest: The authors declare no conflict of interest. The funders had no role in the design of the study; in the collection, analyses, or interpretation of data; in the writing of the manuscript, or in the decision to publish the results.

References

1. Samartzis, P.C.; Wodtke, A.M. All-Nitrogen Chemistry: How Far Are We from N₆₀? *Int. Rev. Phys. Chem.* **2006**, *25*, 527–552. [[CrossRef](#)]
2. Witkowski, T.G.; Richardson, P.; Gabidullin, B.; Hu, A.; Murugesu, M. Synthesis and Investigation of 2,3,5,6-Tetra-(1H-Tetrazol-5-Yl)Pyrazine Based Energetic Materials. *ChemPlusChem* **2018**, *83*, 984–990. [[CrossRef](#)]
3. Zhang, J.; Chen, G.; Gong, X. Screening for Potential Energetic C–N Cages with High Energy and Good Stability: A Theoretical Comparative Study. *Mol. Simul.* **2018**, *45*, 129–136. [[CrossRef](#)]
4. Zhang, Z.; Ma, J.; Zhou, Q.; Hu, W.; Zhang, X. 2-Fluoro-1,3-Diamino-4,6-Dinitrobenzene (ZXC-7) and 2-Fluoro-1,3,5-Triamino-4,6-Dinitrobenzene (ZXC-8): Thermally Stable Explosives with Outstanding Properties. *ChemPlusChem* **2019**, *84*, 119–122. [[CrossRef](#)] [[PubMed](#)]
5. Eremets, M.I.; Gavriliuk, A.G.; Serebryanaya, N.R.; Trojan, I.A.; Dzivenko, D.A.; Boehler, R.; Mao, H.K.; Hemley, R.J. Structural Transformation of Molecular Nitrogen to a Single-Bonded Atomic State at High Pressures. *J. Chem. Phys.* **2004**, *121*, 11296. [[CrossRef](#)]
6. Tomasino, D.; Kim, M.; Smith, J.; Yoo, C.-S. Pressure-Induced Symmetry-Lowering Transition in Dense Nitrogen to Layered Polymeric Nitrogen (LP-N) with Colossal Raman Intensity. *Phys. Rev. Lett.* **2014**, *113*. [[CrossRef](#)]
7. Strout, D.L. Stabilization of an All-Nitrogen Molecule by Oxygen Insertion: Dissociation Pathways of N₈O₆. *J. Phys. Chem. A* **2003**, *107*, 1647–1650. [[CrossRef](#)]
8. Chen, J.; Yu, Y.; Li, Y.; Pang, S. Combination High Energy with Stability: Polynitrogen Explosives N₁₄ and N₁₈. *Phys. Chem.* **2018**. [[CrossRef](#)]
9. Owens, F.J. Density Functional Calculation of Structure and Stability of Nitrogen Clusters N₁₀, N₁₂, and N₂₀. *J. Mol. Struct. THEOCHEM* **2003**, *623*, 197–201. [[CrossRef](#)]
10. Lee, T.J.; Rice, J.E. Theoretical Characterization of Tetrahedral N₄. *J. Chem. Phys.* **1991**, *94*, 1215–1221. [[CrossRef](#)]
11. Li, Q.S.; Liu, Y.D. Theoretical Studies of the N₆Potential Energy Surface. *J. Phys. Chem. A* **2002**, *106*, 9538–9542. [[CrossRef](#)]

12. Chung, G.; Schmidt, M.W.; Gordon, M.S. An Ab Initio Study of Potential Energy Surfaces for N₈Isomers. *J. Phys. Chem. A* **2000**, *104*, 5647–5650. [[CrossRef](#)]
13. Bruney, L.Y.; Bledson, T.M.; Strout, D.L. What Makes an N₁₂ Cage Stable? *Inorg. Chem.* **2003**, *42*, 8117–8120. [[CrossRef](#)]
14. Strout, D.L. Cage Isomers of N₁₄ and N₁₆: Nitrogen Molecules That Are Not a Multiple of Six. *J. Phys. Chem. A* **2004**, *108*, 10911–10916. [[CrossRef](#)]
15. Sturdivant, S.E.; Nelson, F.A.; Strout, D.L. Trends in Stability for N₁₈ Cages. *J. Phys. Chem. A* **2004**, *108*, 7087–7090. [[CrossRef](#)]
16. Strout, D.L. Why Isn't the N₂₀ Dodecahedron Ideal for Three-Coordinate Nitrogen? *J. Phys. Chem. A* **2005**, *109*, 1478–1480. [[CrossRef](#)]
17. Strout, D.L. Isomer Stability of N₂₄, N₃₀, and N₃₆ Cages: Cylindrical versus Spherical Structure. *J. Phys. Chem. A* **2004**, *108*, 2555–2558. [[CrossRef](#)]
18. Silva, M.X.; Silva, F.T.; Galvão, B.R.L.; Braga, J.P.; Belchior, J.C. A Genetic Algorithm Survey on Closed-Shell Atomic Nitrogen Clusters Employing a Quantum Chemical Approach. *J. Mol. Modeling* **2018**, *24*. [[CrossRef](#)]
19. Zhou, H.; Beuve, M.; Yang, F.; Wong, N.-B.; Li, W.-K. Theoretical Investigation on the Cylinder-Shaped N₆₆ Cage. *Comput. Theor. Chem.* **2013**, *1005*, 68–74. [[CrossRef](#)]
20. Zhou, H.; Wong, N.-B.; Zhou, G.; Tian, A. What Makes the Cylinder-Shaped N₇₂ Cage Stable? *J. Phys. Chem. A* **2006**, *110*, 7441–7446. [[CrossRef](#)]
21. Zhou, H.; Wong, N.-B.; Zhou, G.; Tian, A. Theoretical Study on “Multilayer” Nitrogen Cages. *J. Phys. Chem. A* **2006**, *110*, 3845–3852. [[CrossRef](#)] [[PubMed](#)]
22. Wang, L.J.; Zgierski, M.Z. Super-High Energy-Rich Nitrogen Cluster N₆₀. *Chem. Phys. Lett.* **2003**, *376*, 698–703. [[CrossRef](#)]
23. Lee, C.; Yang, W.; Parr, R.G. Development of the Colle-Salvetti Correlation-Energy Formula into a Functional of the Electron Density. *Phys. Rev. B* **1988**, *37*, 785–789. [[CrossRef](#)]
24. Becke, A.D. Density-functional Thermochemistry. III. The Role of Exact Exchange. *J. Chem. Phys.* **1993**, *98*, 5648–5652. [[CrossRef](#)]
25. Krishnan, R.; Binkley, J.S.; Seeger, R.; Pople, J.A. Self-consistent Molecular Orbital Methods. XX. A Basis Set for Correlated Wave Functions. *J. Chem. Phys.* **1980**, *72*, 650–654. [[CrossRef](#)]
26. Schmidt, M.W.; Baldridge, K.K.; Boatz, J.A.; Elbert, S.T.; Gordon, M.S.; Jensen, J.H.; Koseki, S.; Matsunaga, N.; Nguyen, K.A.; Su, S.; et al. General Atomic and Molecular Electronic Structure System. *J. Comput. Chem.* **1993**, *14*, 1347–1363. [[CrossRef](#)]
27. Vineyard, G.H. Frequency Factors and Isotope Effects in Solid State Rate Processes. *J. Phys. Chem. Solids* **1957**, *3*, 121–127. [[CrossRef](#)]
28. Ufimtsev, I.S.; Martinez, T.J. Quantum Chemistry on Graphical Processing Units. 3. Analytical Energy Gradients, Geometry Optimization, and First Principles Molecular Dynamics. *J. Chem. Theory Comput.* **2009**, *5*, 2619–2628. [[CrossRef](#)]
29. Titov, A.V.; Ufimtsev, I.S.; Luehr, N.; Martinez, T.J. Generating Efficient Quantum Chemistry Codes for Novel Architectures. *J. Chem. Theory Comput.* **2012**, *9*, 213–221. [[CrossRef](#)]
30. Kästner, J.; Carr, J.M.; Keal, T.W.; Thiel, W.; Wander, A.; Sherwood, P. DL-FIND: An Open-Source Geometry Optimizer for Atomistic Simulationst. *J. Phys. Chem. A* **2009**, *113*, 11856–11865. [[CrossRef](#)]
31. Goumans, T.P.M.; Catlow, C.R.A.; Brown, W.A.; Kästner, J.; Sherwood, P. An Embedded Cluster Study of the Formation of Water on Interstellar Dust Grains. *Phys. Chem. Chem. Phys.* **2009**, *11*, 5431–5436. [[CrossRef](#)]
32. Allen, M.P.; Tildesley, D.J. *Computer Simulation of Liquids*; Oxford University press: New York, NY, USA, 1991; ISBN 978-0198556459.
33. Chemcraft-Graphical Software for Visualization of Quantum Chemistry Computations. Available online: <https://www.chemcraftprog.com> (accessed on 12 October 2020).
34. Giannozzi, P.; Baroni, S.; Bonini, N.; Calandra, M.; Car, R.; Cavazzoni, C.; Ceresoli, D.; Chiarotti, G.L.; Cococcioni, M.; Dabo, I.; et al. QUANTUM ESPRESSO: A Modular and Open-Source Software Project for Quantum Simulations of Materials. *J. Phys. Condens. Matter* **2009**, *21*, 395502. [[CrossRef](#)]
35. Giannozzi, P.; Andreussi, O.; Brumme, T.; Bunau, O.; Buongiorno Nardelli, M.; Calandra, M.; Car, R.; Cavazzoni, C.; Ceresoli, D.; Cococcioni, M.; et al. Advanced Capabilities for Materials Modelling with Quantum ESPRESSO. *J. Phys. Condens. Matter* **2017**, *29*, 46. [[CrossRef](#)]

36. Perdew, J.P.; Burke, K.; Ernzerhof, M. Generalized Gradient Approximation Made Simple. *Phys. Rev. Lett.* **1996**, *77*, 3865–3868. [[CrossRef](#)]
37. Blöchl, P.E. Projector Augmented-Wave Method. *Phys. Rev. B* **1994**, *50*, 17953–17979. [[CrossRef](#)]
38. Kresse, G.; Joubert, D. From Ultrasoft Pseudopotentials to the Projector Augmented-Wave Method. *Phys. Rev. B* **1999**, *59*, 1758–1775. [[CrossRef](#)]
39. Grimme, S.; Antony, J.; Ehrlich, S.; Krieg, H. A Consistent and Accurate Ab Initio Parametrization of Density Functional Dispersion Correction (DFT-D) for the 94 Elements H–Pu. *J. Chem. Phys.* **2010**, *132*, 154104. [[CrossRef](#)]
40. Monkhorst, H.J.; Pack, J.D. Special Points for Brillouin-Zone Integrations. *Phys. Rev. B* **1976**, *13*, 5188–5192. [[CrossRef](#)]
41. Methfessel, M.; Paxton, A.T. High-Precision Sampling for Brillouin-Zone Integration in Metals. *Phys. Rev. B* **1989**, *40*, 3616–3621. [[CrossRef](#)]
42. Blöchl, P.E.; Jepsen, O.; Andersen, O.K. Improved Tetrahedron Method for Brillouin-Zone Integrations. *Phys. Rev. B* **1994**, *49*, 16223–16233. [[CrossRef](#)] [[PubMed](#)]
43. Kroto, H.W. The Stability of the Fullerenes C_n, with n = 24, 28, 32, 36, 50, 60 and 70. *Nature* **1987**, *329*, 529–531. [[CrossRef](#)]
44. Schwerdtfeger, P.; Wirz, L.; Avery, J. Program Fullerene: A Software Package for Constructing and Analyzing Structures of Regular Fullerenes. *J. Comput. Chem.* **2013**, *34*, 1508–1526. [[CrossRef](#)]
45. Tománek, D. *Guide through the Nanocarbon Jungle: Buckyballs, Nanotubes, Graphene, and Beyond*; Morgan & Claypool Publishers: San Rafael, CA, USA, 2014. [[CrossRef](#)]
46. Grishakov, K.; Katin, K.; Gimaldinova, M.; Maslov, M. Stability and Energy Characteristics of Extended Nitrogen Nanotubes: Density Functional Theory Study. *Lett. Mater.* **2019**, *9*, 366–369. [[CrossRef](#)]
47. Gimaldinova, M.A.; Zemenkov, L.I.; Merinov, V.A. Stabilization of Small Nitrogen Clusters via Spatial Constraint. *J. Phys. Conf. Ser.* **2020**, *1435*, 012062. [[CrossRef](#)]
48. Gimaldinova, M.A.; Katin, K.P.; Grishakov, K.S.; Maslov, M.M. Kinetic Stability of Nitrogen Cubane inside the Fullerene Cage: Molecular Dynamics Study. *Fuller. Nanotub. Carbon Nanostruct.* **2019**, *28*, 304–308. [[CrossRef](#)]
49. Greschner, M.J.; Zhang, M.; Majumdar, A.; Liu, H.; Peng, F.; Tse, J.S.; Yao, Y. A New Allotrope of Nitrogen as High-Energy Density Material. *J. Phys. Chem. A* **2016**, *120*, 2920–2925. [[CrossRef](#)]
50. Li, Y.; Feng, X.; Liu, H.; Hao, J.; Redfern, S.A.T.; Lei, W.; Liu, D.; Ma, Y. Route to High-Energy Density Polymeric Nitrogen t-N via He–N Compounds. *Nat. Commun.* **2018**, *9*. [[CrossRef](#)]
51. Bondarchuk, S.V.; Minaev, B.F. Super High-Energy Density Single-Bonded Trigonal Nitrogen Allotrope—A Chemical Twin of the Cubic Gauche Form of Nitrogen. *Phys. Chem. Chem. Phys.* **2017**, *19*, 6698–6706. [[CrossRef](#)]
52. Adeleke, A.A.; Greschner, M.J.; Majumdar, A.; Wan, B.; Liu, H.; Li, Z.; Gou, H.; Yao, Y. Single-Bonded Allotrope of Nitrogen Predicted at High Pressure. *Phys. Rev. B* **2017**, *96*. [[CrossRef](#)]
53. Maslov, M.M.; Katin, K.P. On the Thermal Stability of Tetrahedrane: Tight-Binding Molecular Dynamics Study. *Chem. Phys.* **2011**, *387*, 66–68. [[CrossRef](#)]
54. Katin, K.P.; Prudkovskiy, V.S.; Maslov, M.M. Influence of Methyl Functional Groups on the Stability of Cubane Carbon Cage. *Phys. E Low-Dimens. Syst. Nanostruct.* **2016**, *81*, 1–6. [[CrossRef](#)]
55. Oganov, A.R.; Glass, C.W. Crystal Structure Prediction Using ab Initioevolutionary Techniques: Principles and Applications. *J. Chem. Phys.* **2006**, *124*, 244704. [[CrossRef](#)]
56. Wang, Y.; Lv, J.; Zhu, L.; Ma, Y. CALYPSO: A Method for Crystal Structure Prediction. *Comput. Phys. Commun.* **2012**, *183*, 2063–2070. [[CrossRef](#)]
57. Xiong, W. A Simole Method for Calculating Detonation Parameters of Explosives. *J. Energ. Mater.* **1985**, *3*, 263–277. [[CrossRef](#)]
58. Yan, Q.-L.; Zeman, S. Theoretical Evaluation of Sensitivity and Thermal Stability for High Explosives Based on Quantum Chemistry Methods: A Brief Review. *Int. J. Quantum Chem.* **2012**, *113*, 1049–1061. [[CrossRef](#)]
59. Kim, C.; Cho, S.-G.; Kim, C.K.; Lee, H.W. QSPR Studies on Impact Sensitivities of High Energy Density Molecules. *Bull. Korean Chem. Soc.* **2011**, *32*, 4341–4346. [[CrossRef](#)]

60. Rice, B.M.; Hare, J.J. A Quantum Mechanical Investigation of the Relation between Impact Sensitivity and the Charge Distribution in Energetic Molecules. *J. Phys. Chem. A* **2002**, *106*, 1770–1783. [[CrossRef](#)]
61. Simpson, R.L.; Urtiew, P.A.; Ornellas, D.L.; Moody, G.L.; Scribner, K.J.; Hoffman, D.M. CL-20 Performance Exceeds That of HMX and Its Sensitivity Is Moderate. *Propellants Explos. Pyrotech.* **1997**, *22*, 249–255. [[CrossRef](#)]

Publisher's Note: MDPI stays neutral with regard to jurisdictional claims in published maps and institutional affiliations.



© 2020 by the authors. Licensee MDPI, Basel, Switzerland. This article is an open access article distributed under the terms and conditions of the Creative Commons Attribution (CC BY) license (<http://creativecommons.org/licenses/by/4.0/>).